

Estimating energy levels from lattice QCD correlation functions using a transfer matrix formalism

Debsubhra Chakraborty ^{1,*} Dhruv Sood ^{1,†} Archana Radhakrishnan ^{1,‡} and Nilmani Mathur ^{1,§}

¹*Department of Theoretical Physics, Tata Institute of Fundamental Research,
Homi Bhabha Road, Mumbai 400005, India*

We present an efficient method for estimating energy levels from lattice QCD correlation functions by computing the eigenvalues of the transfer matrix of the corresponding lattice QCD Hamiltonian. This method is equivalent to the Lanczos procedure introduced recently [1], but more general and simpler to implement. We demonstrate the efficacy of the method by calculating the two lowest energy levels of a large number of hadrons including a few nuclei. While the signal-to-noise problem does not improve significantly, the extracted energy levels are found to be more reliable, compared to those extracted by conventional methods. Within a given statistical dataset the proposed method can effectively account for both statistical uncertainties and systematic errors, including those arising from the fitting window, and hence can reliably be employed in lattice QCD calculations.

I. INTRODUCTION

Extraction of energy levels from two-point correlation functions is an essential component in most lattice QCD studies. The methods involved in that need to be reliable and efficient not only for determining the energy spectra accurately but also for probing and understanding the internal structures of hadrons, particularly for any precision study. In general, by exploiting the asymptotic decay of two-point correlation functions, $C(\tau) \sim e^{-E_n\tau}$, one can extract the ground state, E_0 , at a sufficiently large distances from its source of excitation ($\tau \rightarrow \infty$). Over the years, better methodologies for extracting energy levels have been developed within the framework of the generalized eigenvalue problem (GEVP) [2, 3]. These approaches use a large variational basis of interpolating fields to estimate the energy levels more reliably. All these methods have produced remarkable results, particularly for stable hadrons [4, 5], achieving per-mille accuracy in many cases and even predicting subatomic particles before their experimental discovery [6–8]. More recently, these methods have also been extensively applied to study resonance properties and scattering phenomena [9]. However, a significant challenge in these procedures remains the signal-to-noise-ratio (SNR) problem in Euclidean correlation functions, as pointed out by Parisi [10] and Lepage [11]. This issue, intrinsic to lattice QCD calculations, becomes more pronounced for systems involving multi-hadron states, and becomes a hindrance particularly for nuclei [12–15]. Overcoming this bottleneck remains a key focus in improving the precision and reliability of lattice QCD studies.

Recently, an alternative procedure has been introduced [1, 16] based on computation of eigenvalues of the transfer matrix. Since the transfer matrix is infinite dimensional, a

recursive procedure using Lanczos method was employed, leveraging Kaniel-Paige-Saad (KPS) bound on energy estimation [17, 18]. The efficacy of the above method was shown using toy model calculations as well as for pion and nucleon. However, as noted there, a major challenge with this method is filtering out spurious eigenvalues, which can introduce subjectivity and systematic errors into the estimation of energy levels.

Following this development, here we propose a similar method to estimate the energy levels from the eigenvalues of the transfer matrix. Specifically, we employ another Krylov space-based method for eigenvalue extraction from two-point correlation functions of lattice QCD ¹. Our method is straightforward to implement and can be seamlessly extended to the generalized eigenvalue problem (GEVP) [2, 3], offering enhanced simplicity and ease of implementation. We employ a variation of the Prony generalized eigenvalue method [20–23], and we refer this method as Transfer matrix GEVP (TGEVP). We demonstrate the potency of the method by extracting the two lowest eigenvalues from the various two-point functions of a variety of hadrons, including nuclei. Similar to Ref. [19] we also find that the energy estimates obtained with this method are identical to those derived using the oblique Lanczos algorithm outlined in [1]. Below we describe the method.

II. METHODOLOGY

In lattice QCD calculations, a two-point correlation function, corresponding to an interpolating field \mathcal{O} , between a source (\mathbf{x}_i, t_i) and sink (\mathbf{x}_f, t_f) is given by,

$$C(t = t_f - t_i) = \sum_{\mathbf{x}} \langle \Omega | \mathcal{O}(\mathbf{x}_f, t_f) \bar{\mathcal{O}}(\mathbf{x}_i, t_i) | \Omega \rangle, \quad (1)$$

¹ During the final stage of drafting this article, another article was published on arXiv (Ref. [19]), which also utilized the similar method as in this work. However, we used a different filtering procedure of eigenvalues and the error estimation is also different.

* debsubhra.chakraborty@tifr.res.in

† dhruv.sood@tifr.res.in

‡ archana.radhakrishnan@tifr.res.in

§ nilmani@theory.tifr.res.in

where $|\Omega\rangle$ represents the vacuum state of the theory. In terms of the Hamiltonian matrix \mathcal{H} , in general we also express a two-point function as,

$$C(t) = \langle \Omega | \mathcal{O}(0) e^{-\hat{\mathcal{H}}t} \bar{\mathcal{O}}(0) | \Omega \rangle, \quad (2)$$

If $\hat{\mathcal{T}} \equiv e^{-\hat{\mathcal{H}}}$ is the transfer matrix in Euclidean space-time, in terms of the states, $|\chi\rangle \equiv \bar{\mathcal{O}}(0)|\Omega\rangle$ created by the interpolating field, we can write the above expression as,

$$C(t) = \langle \chi | \hat{\mathcal{T}}^t | \chi \rangle. \quad (3)$$

In lattice QCD simulations, however, $C(t)$ is computed only at a finite number of discrete times, specifically at $t \in a, 2a, \dots, n_T a$, where a is the lattice spacing and n_T is the temporal extent of the lattice. This leads to

$$C(na) = \langle \chi | \hat{\mathcal{T}}^{na} | \chi \rangle, \text{ where } n \in 1, 2, \dots, n_T. \quad (4)$$

For simplicity, we assume the lattice units to be $a = 1$, reducing the above equation to,

$$C(n) = \langle \chi | \hat{\mathcal{T}}^n | \chi \rangle. \quad (5)$$

The eigenvalues of the transfer matrix corresponds to the eigenstates of the Hamiltonian \mathcal{H} . Usually, while the transfer matrix is infinite dimensional, in classical computation one always needs to work with a truncated transfer matrix evaluated on a finite-dimensional basis. Here we choose the vectors in Krylov-subspace, \mathcal{K}_m , as a set of linearly-independent basis vectors, which are given below,

$$\mathcal{K}_m \equiv \{|\chi\rangle, \hat{\mathcal{T}}|\chi\rangle, \hat{\mathcal{T}}^2|\chi\rangle, \dots, \hat{\mathcal{T}}^m|\chi\rangle\}, \quad (6)$$

for $2m - 1 \leq n_T$.

Since this set of vectors is neither orthogonal nor normalized, we normalize those as, $|v_i\rangle = \hat{\mathcal{T}}^i|\chi\rangle / \sqrt{\langle \chi | \hat{\mathcal{T}}^{2i} | \chi \rangle}$. Next, in terms of these basis vectors $|v_i\rangle$ s we define following two-matrices,

$$T_{ij}^m = \langle v_i | \hat{\mathcal{T}} | v_j \rangle = \frac{C(i+j+1)}{\sqrt{C(2i)C(2j)}} \quad \text{for } 0 \leq i, j \leq m \quad (7)$$

$$V_{ij}^m = \langle v_i | v_j \rangle = \frac{C(i+j)}{\sqrt{C(2i)C(2j)}} \quad \text{for } 0 \leq i, j \leq m \quad (8)$$

It can be shown that the eigenvalues of $\hat{\mathcal{T}}$ matrix, truncated in the Krylov-subspace \mathcal{K}_m , can be obtained by solving the following generalized eigenvalue problem (GEVP),

$$T^m x_n^m = \lambda_n^m V^m x_n^m, \quad \text{for } 0 \leq n \leq m, \quad (9)$$

where λ_n^m 's and x_n^m 's are eigenvalues and eigenvectors of the transfer matrix truncated on the $(m+1)$ dimensional Krylov-subspace (we provide the proof in the Appendix A). Note that, V^m and T^m both are positive-definite matrices for a given source-sink setup. Hence the eigenvalues, λ_n^m , in Eq. (9) are real and positive. The energies of the eigenstates of the truncated transfer matrix are given by,

$E_n^m = -\log \lambda_n^m$. Since the eigenenergies are positive, we expect $0 \leq \lambda_n^m \leq 1$ ².

Note that for the case of staggered quarks, the two-point correlation functions will have contribution from opposite parity states with an oscillating phase in time $(-1)^t$. Consequently, along with the positive eigenvalues, there are negative real eigenvalues, λ_n^o , corresponding to the oscillating term of the correlation functions. They will corresponds to energy, $E_n^o = -\log \lambda_n^o + i\pi = -\log(|\lambda_n^o|)$, with a phase $(-1)^t$. We will elaborate this while presenting results with staggered quarks. Similarly, for a thermal correlator the eigenvalues will be complex and a separate method is needed to gain information on thermal modes. However, that is beyond the scope of this work.

In the absence of statistical noise in a correlation function, $C(n)$, selecting eigenvalues across different iterations of the matrix T^m is straightforward. The eigenvalues computed in the m -th iteration will be arranged in increasing order, $E_0^m < E_1^m < E_2^m < \dots < E_m^m$, where E_0^m represents the ground-state energy estimate for the m -th iteration, while E_i^m for $1 \leq i \leq m$ corresponds to the subsequent excited states. In lattice QCD simulations, however, the correlation functions are evaluated stochastically using the Monte Carlo path integral approach with finite statistics. This introduces statistical noise, causing fluctuations in the computed matrices C^m and T^m which can then deviate from their positive-definite structure, resulting spurious eigenvalues in the spectrum of the T^m . This issue is particularly problematic in systems with a dense spectrum, as the spurious eigenvalues can disrupt the proper ordering of energy levels, making the extraction of reliable energy levels challenging. This issue has already been pointed out in Ref. [1], where a filtering procedure with Cullum-Willoughby method [24] was employed to eliminate these spurious eigenvalues. However, as noted there, such filtering procedure provides only a partial solution to the problem which can make the eigenvalue estimation, particularly their errors, unreliable.

A. Procedure for spurious eigenvalue filtration

To address the issue of spurious eigenvalues, we employ a pivoting technique that iteratively refines the eigenvalue histogram by weighting high-confidence peaks based on Gaussian filtering and full-width half-maximum criteria. Below, we outline the steps involved in the eigenvalue filtration process:

1. First, we perform bootstrap resampling on the original dataset to generate N_b bootstrap samples. For each of these samples, we carry out GEVP calculations, as defined in Eq. (9), and compute the energy eigenvalues $\lambda_n^{m,b}$. Here, the index n enumerates the eigenvalues obtained for the

² As, described in [1], thermal states appear in the spectrum of \mathcal{T}^m with $\lambda_n^m > 1$. However we are not interested in these states here.

m -th iteration and the b -th bootstrap sample. The ranges are defined as $0 \leq n \leq m$, $1 \leq m \leq \lfloor (N_T + 1)/2 \rfloor$, and $b \in \{1, 2, \dots, N_b\}$.

2. Next, we eliminate all eigenvalues with $|\arg \lambda_n^{m,b}| > \epsilon$, retaining only the real eigenvalues (value of ϵ depends on the required precision). Eigenvalues outside the range $0 < \lambda \leq 1$ are discarded, as they do not correspond to physically meaningful energy states. For staggered valence quarks, however, because of the oscillating states, one needs to include eigenvalues in the range $\lambda_n^{m,b} \in (-1, 0)$.

3. For each iteration, a histogram is generated from the eigenvalues obtained across all bootstrap samples. To reduce statistical fluctuations in the histogram, smoothing techniques such as Gaussian filtering are utilized. The peaks in the histogram are then identified by determining their centers and calculating their full width at half maximum (FWHM). These peak-centers and their corresponding widths are denoted by C_r^m and Δ_r^m , respectively, where m refers to the iteration number, and the subscript r indexes the peaks in descending order of their center values. This approach allows for a clearer identification of dominant eigenvalues. An example plot demonstrating this process is provided in Appendix D.

4. Each peak thus identified in the histogram represents an eigenstate of the transfer matrix. The peak-centers and their widths are then utilized to guide the pivoting procedure for selecting eigenvalues, ensuring that only physically meaningful eigenstates are retained. This procedure enhances the reliability of the extracted energy levels by systematically filtering out spurious eigenvalues and maintaining a consistent ordering of eigenvalues.

5. For each peak in the m -th iteration, we select the eigenvalue $\lambda_n^{m,b}$ that is closest to C_r^m and lies within the range $[C_r^m - \Delta_r^m, C_r^m + \Delta_r^m]$ for each bootstrap sample. This procedure results in a set of filtered eigenvalues, denoted as $\tilde{\lambda}_r^{m,b}$, where the index r represents the peaks in the histogram, or equivalently, the well-resolved states in the spectrum of T^m . For instance, $-\log \tilde{\lambda}_{r=0}^{m,b}$ represents the ground-state energy eigenvalue for the m -th iteration and the b -th bootstrap sample.

Naturally, a concern here is on the accurate estimation of errors in the eigenvalues obtained using the above procedure, particularly when comparing them with effective masses. One needs to account for the potential influence of outliers in the bootstrap eigenvalue estimates. In Refs. [1, 19] a double-bootstrap method was utilized to address that. Instead, we adopt the 68th percentile as the bootstrap confidence interval. Despite the filtration procedure applied to the eigenvalues $\tilde{\lambda}_r^{m,b}$, some outliers may still remain. These outliers can skew the bootstrap mean and inflate the bootstrap standard error, particularly in certain iterations. To mitigate this, we define the bootstrap confidence interval by using the 68th percentile, which corresponds to the interval between the 16th and 84th percentiles of the bootstrap distribution.

The mean of the eigenvalues within this 68th percentile interval is then quoted as the bootstrap mean. However, to be conservative with errors, we estimate those using the 68th percentile of the *full samples* without removing any outlier. We find this approach reduces the influence of extreme values robustly with reliable errorbars, leading to more stable and robust estimates. We automate the whole procedure described above after fixing the count-threshold for peak detection and the smoothing-parameter of the histogram counts, thus reducing subjectiveness and associated systematics.

III. RESULTS

We now present the results as obtained by the aforementioned TGEVP method. Eigenvalues are computed using two different approaches, namely by PYTHON [25] and FEAST eigensolvers [26], ensuring cross-checking while maintaining high precision evaluation. In Figs. [1, 2, 3, 4] we show our results. In each of the figures we present the lowest eigenvalue as estimated by the above method, along with the standard effective mass, defined as $m_{eff}(t) = \log[C(t)/C(t+1)]$. In each case, throughout this article, blue circles represent the regular effective mass $m_{eff}(t)$, and the red circles represent the lowest eigenvalues as computed over the iterations. The magenta band represents the correlated fit of the two-point function using a single exponential, illustrating the fit range and the associated 1σ error. The faded-green band corresponds to the eigenvalues, fitted with a constant term over multiple iterations, also using a correlated fit. This comparison highlights the stability and error behavior of the TGEVP eigenvalues over regular effective mass approach. A large number of other results, including the first excited states, are shown in Appendix C and are discussed there.

A. Case I: Charmonia

We first present the results for the 1S-charmonia in Fig. 1. The results corresponds to the two-point correlation functions of 0^- (top) and 1^- (bottom) states of charmonia, as computed using overlap valence quarks with a HISQ lattice ensemble ($48^3 \times 144$, $a = 0.0582$ fm, $n_{meas} = 180$). As can be observed, while the effective mass is fluctuating over time-slices, the lowest eigenvalue estimated over different iterations is very stable. In Appendix C, we further show similar results for other lattice ensembles along with the first excited states. We also show the continuum extrapolation of mass splittings between the excited and the ground states, and compare those with their experimental values.

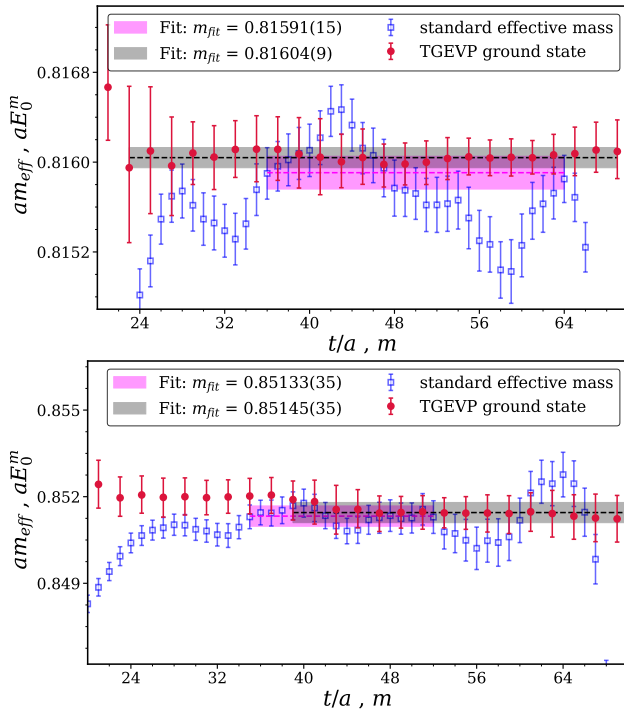


FIG. 1. Comparison of the results between the standard effective mass of the ground state (blue circles) and the lowest eigenvalue (red circles) corresponding to the two-point correlation functions of the pseudoscalar ($J^P \equiv 0^-$) (top) and vector (1^-) (bottom) states of charmonia. Number of measurements (n_{meas}) in this case is 180.

B. Case II: Heavy Baryons

In Fig. 2, we show similar results obtained from two-point correlation functions of the heavy baryon Ξ_{cc} , at two different quark masses. It again very clearly shows the stability of the lowest eigenvalue over the iteration numbers, as opposed to unstable and fluctuating effective mass data. In such cases, the TGEVP results can really be helpful to extract the ground state, avoiding systematic uncertainty due to various choices of fit ranges in the regular fitting procedures.

C. Case III: Nucleon

In Fig. 3, we show similar results obtained from a smeared-point two-point function of the nucleon computed at a near physical pion mass. While the results from the two estimations are consistent, the eigenvalues at the larger iterations have smaller errors compared to errors in the effective mass at the larger times.

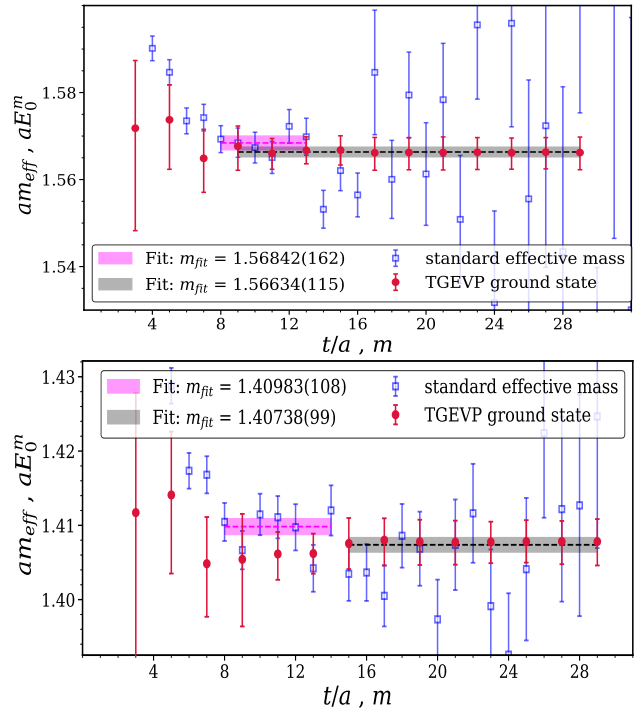


FIG. 2. Similar to Fig. 1, corresponding to smeared-smeared two-point functions for the doubly charmed baryon Ξ_{cc} , computed at two different light quark masses with number of measurements (n_{meas}) 1612 and 2000 respectively.

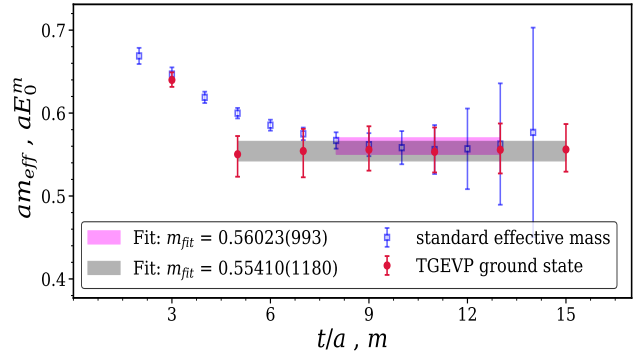


FIG. 3. Similar to Fig. 1, corresponding to a smeared-point two-point function of nucleon ($n_{meas} = 300$)

D. Case IV: Nuclei

One of the main bottlenecks in lattice QCD studies of nuclei is the lack of reliability in extracting the energy levels, even for the ground states of low-lying nuclei [12–15]. This is primarily due to poor signal-to-noise ratio in the two-point correlation functions at lighter quark masses, resulting very noisy and small plateau at a large distance in the effective mass plots. As a result, statistical error together with fit-uncertainties, becomes large making the whole process unreliable. It is thus quite important to check if TGEVP method can be helpful

in this. In Fig. 4, we show the effective mass of the ground state and lowest eigenvalue of TGEVP spectrum for a few nuclei. These results are for ${}^2\text{H}$ (top), ${}^3\text{He}$ (middle) and ${}^4\text{He}$ (bottom) (more such results are shown in Appendix C). The two-point functions are obtained with overlap valence quarks on the $N_f = 2 + 1 + 1$ HISQ gauge ensembles ($48^3 \times 144$, $a = 0.0582$ fm) at the quark masses, $m_u = m_d = m_s$. The method for computing the correlation functions for these nuclei has been provided in Ref. [15]. As can be observed that the effective masses of these nuclei exhibit significant noise from the start, requiring substantial systematic error corrections in traditional fitting methods. In contrast, the TGEVP eigenvalues remain stable across numerous iterations. With a large number of measurements, it is expected that the errors in eigenvalues in each iteration can be reduced. However, it is also necessary to assess the method's effectiveness for the cases with closely spaced states carrying finite momentum, particularly when dealing with varied source-sink setups in nuclear systems. Another point of concern is correlation over iterations which we will discuss next. Nevertheless, as the results suggest, this method holds excellent promise for extracting reliable energy levels for nuclei in the future.

E. Correlation in TGEVP eigenvalues

A natural concern is for accounting the correlation between eigenvalues obtained across iterations and the validity of a constant fit over iterations. Addressing this correlation mathematically, where data in each step in a matrix are generated randomly from the previous step, is non-trivial. In Refs. [1, 19] a double-bootstrapping is done to address that. In this work, we define the bootstrap confidence interval by using the 68th percentile. To assess the extent of correlation, we define the correlation matrix under bootstrap and compute that for the eigenvalues that lies within the 68th percentile interval. In Fig. 5, we show such a color-coded correlation-plot for the two-point correlation functions for η_c that was shown in the top pane of Fig. 1. As observed, the correlation of eigenvalues across iterations is insignificant at the beginning and increases towards the end. Particularly in the fit region (Fig. 1), it remains small enough to justify a correlated fitting with a constant term. Additional examples are provided in the Appendix E, showing smaller correlations for most datasets, except for nuclei where relatively larger correlations are observed. For nuclei, however, while this method does not solve the SNR problem, it mitigates that to an extent and provides a more reliable estimation of the energy levels compared to existing fitting methods.

IV. CONCLUSION AND OUTLOOK

This work presents an efficient method for extracting energy levels by applying generalized eigenvalue frame-

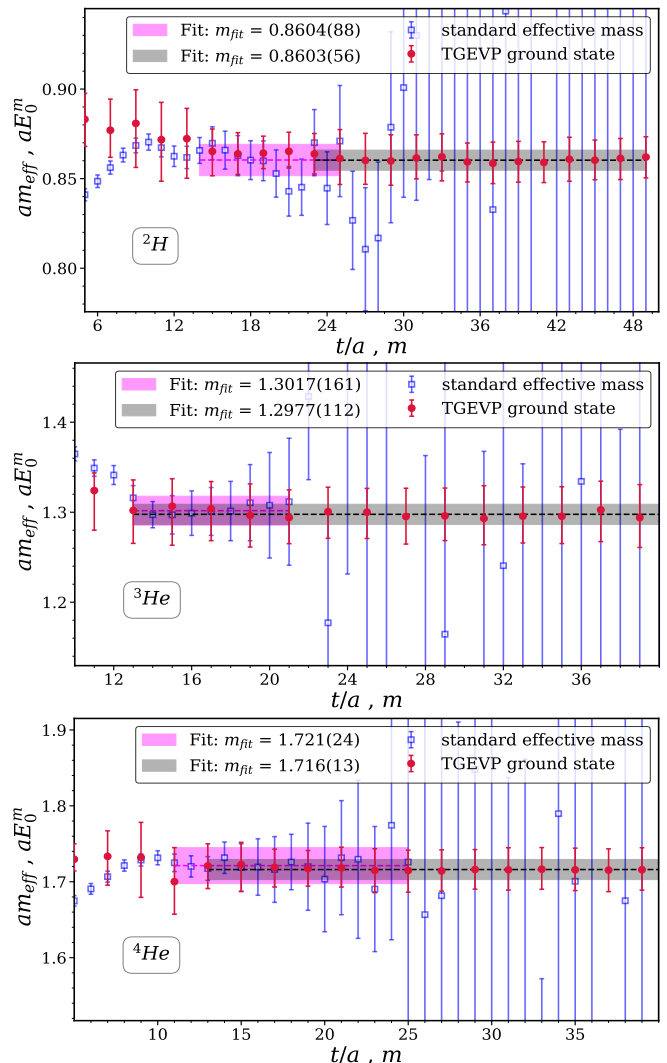


FIG. 4. Comparison of the results between the regular effective mass (blue circles) and TGEVP ground state (red circles) corresponding to two-point functions of a few light nuclei. Top: ${}^2\text{H}$, middle: ${}^3\text{He}$, and bottom: ${}^4\text{He}$, with the quark masses, $m_u = m_d = m_s$ ($n_{\text{meas}} = 168$).

work to the transfer matrix constructed from time-shifted two-point correlation functions of lattice QCD. We find this method is equivalent, both analytically as well as numerically, to the Lanczos method [1], but is more general and easy to implement. A pivoting procedure, along with a bootstrap confidence interval of 68th percentile, is employed for removing spurious eigenvalues, and is found to be more efficient than the Cullum-Willoughby method. We demonstrate the efficacy of the method by calculating first two eigenvalues from two-point functions of a variety of hadrons, including nuclei. For charmonia, along with the individual energy levels we also compute energy splittings between different states and show that, when extrapolated to the continuum limit, they align well with experimental values, even with limited statistics. In most cases with higher statistics, we find the correla-

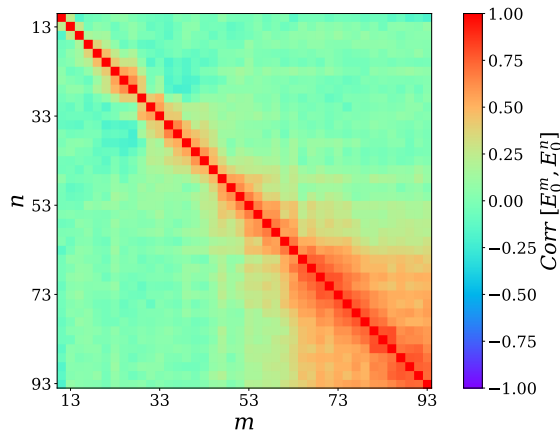


FIG. 5. Color-coded correlation matrix showing the correlations between the eigenvalues across iterations. This dataset corresponds to the two-point correlation functions of the lowest 0^- state (η_c meson), showed in the top pane of Fig. 1.

tion between eigenvalues across iterations is sufficiently low, allowing for a constant fit, which yields more reliable results than traditional exponential fitting methods. For nuclei, we find the correlation between eigenvalues across iterations to be higher than that for single nucleons, particularly when statistics are low. The increased correlation poses a challenge for solving the SNR problem, and a thorough evaluation is necessary to account this correlation for accurate estimation of energy levels in such cases. However, within the limit of a given statistics, the TGEVP eigenvalues remain more stable across iterations compared to the noisy effective masses obtained through traditional methods. This stability suggests that with increased statistics, the use of a multi-operator setup, and proper accounting of correlations, this procedure holds promise for accurately determining energy levels even in challenging multi-nucleon systems.

ACKNOWLEDGMENT

This work is supported by the Department of Atomic Energy, Government of India, under Project Identification Number RTI 4002. Computations related to some of the correlators were done on the Cray-XC30 of ILGTI, TIFR (which has recently been closed), and the computing clusters at the Department of Theoretical Physics, TIFR, Mumbai. NM is thankful to Keh-Fei Liu, Gunnar Bali and Wolfgang Soeldner for providing us with the nucleon, and heavy baryon data. NM and DC also acknowledge discussions with Piyush Srivastava at various stages of this work. We would also like to thank Ajay Salve, Kapil Ghadiali, and T. Chandramohan for computational support.

Appendix A: Equivalence between Lanczos and TGEVP methods

Assuming $|u_i\rangle$, $i = 0, 1, \dots, m$, form a complete set of orthonormal basis in the Krylov-subspace \mathcal{K}_m , the vectors $|v_i\rangle$, that enter in Eqs. (7) and (8), can be expanded as,

$$|v_i\rangle = \sum_{j=0}^m \alpha_{ij} |u_j\rangle. \quad (\text{A1})$$

The eigenvalue equation for the transfer matrix \mathcal{T} using this orthonormal basis $|u_i\rangle$'s is given by,

$$\tilde{T}_{ij}(\tilde{x}_n)_j = \lambda_n(\tilde{x}_n)_i \quad \text{for } 0 \leq n < m, \quad (\text{A2})$$

$$\text{where } \tilde{T}_{ij} = \langle u_i | \mathcal{T} | u_j \rangle.$$

We need to show that the above generalized eigenvalue problem is exactly equivalent to the eigenvalue problem in Eq. (A2). Starting with (9), this equivalence can be demonstrated through the following steps,

$$T_{ij}(x_n)_j = \lambda_n V_{ij}(x_n)_j, \quad (\text{A3})$$

$$\alpha_{ik}^* \tilde{T}_{kl} \alpha_{jl}(x_n)_j = \lambda_n \alpha_{ik}^* \alpha_{jk}(x_n)_j, \quad (\text{A4})$$

$$(\alpha^{-1})_{pi}^* \alpha_{ik}^* \tilde{T}_{kl} \alpha_{jl}(x_n)_j = \lambda_n (\alpha^{-1})_{pi}^* \alpha_{ik}^* \alpha_{jk}(x_n)_j \quad (\text{A5})$$

$$\tilde{T}_{il} \alpha_{jl}(x_n)_j = \lambda_n \alpha_{ji}(x_n)_j, \quad (\text{A6})$$

$$\tilde{T}_{ij}(\tilde{x}_n)_j = \lambda_n(\tilde{x}_n)_i \quad \text{proved.} \quad (\text{A7})$$

Here, in the second step, we have substituted $|v_i\rangle$ utilizing Eq. (A1). In the third step, we have multiplied the both sides of the equation using inverse of α_{ij} (given that $|v_i\rangle$ are linearly-independent, inverse of the matrix α_{ij} exists.). In the final step, we have redefined $(\tilde{x}_n)_i = \alpha_{ji}(x_n)_j$ to arrive at the desired form.

Appendix B: Numerical comparison between Lanczos and TGEVP methods

Below we compare the numerical results obtained with the Lanczos method, as described in [1], and the TGEVP method, as proposed here. We follow a similar implementation of Oblique Lanczos method (Lanczos A) as in Ref. [1]. We also use another method (Lanczos B) which is similar to Ref. [1], except differences in the procedure of filtering and sorting the eigenvalues. We outline the implementation below.

1. We first resample our data to obtain N_b bootstrap samples and perform M iterations of Oblique Lanczos for each, obtaining $\lambda_n^{m,b}$. The index $1 \leq M$ and $1 \leq b \leq N_b$ correspond to Lanczos iterations and the bootstrap sample being used respectively, while n enumerates the computed eigenvalues.

2. Of these $\lambda_n^{m,b}$, we discard all results satisfying $\arg \lambda_n^{m,b} > \epsilon$ with $\epsilon > 10^{-12}$ as spurious. We also discard $\lambda_n^{m,b} > 1$, for reasons described earlier.

3. For each Lanczos iteration, we plot a histogram of the bootstrap eigenvalues and use a Gaussian filter to smoothen the data. We then identify the peaks P_n^m , and their corresponding widths Δ_n^m , in this histogram and sort the $\lambda_n^{m,b}$ on the basis of the peak they correspond to. Iterations where no eigenvalue aligns with a particular peak are treated as though no result is obtained, and so any apparent outliers are discarded. This ensures that only eigenvalues corresponding to the same state are compared or binned together in subsequent analysis, reducing the risk of contamination from spurious or unrelated states.

4. Lanczos A: To these eigenvalues, we apply the Cullum-Willoughby procedure with a threshold ϵ_{CW} . This is utilized to filter out spurious eigenvalues, using the criteria and parameters described in Ref. [1]. This leads to the eigenvalues λ_n^m .

5. Lanczos B: For the mean and error estimation, as in the case of TGEVP, we further use the 68th-percentile bootstrap confidence interval of the eigenvalues obtained in the previous step.

In Fig. 6, we compare the eigenvalues obtained using the Lanczos and TGEVP methods for the η_c and Ξ_{cc} , corresponding to the dataset shown in the respective top panes of Figs. 1 and 2. This comparison suggests the numerical equivalence of the two methods.

Appendix C: Additional results

In addition to the results presented in the main section, here we present more such results for various hadrons including their excited states. In Fig. 7, we show the first two eigenvalues as determined employing TGEVP method. These dataset corresponds to 1S-charmonia states, where the left panel is for 0^- and the right one corresponds to 1^- states. The regular effective mass, $m_{eff}(t)$ is also shown (blue circles) to compare that with the lowest eigenvalue (red circles). In addition to the lowest eigenvalue we find the second eigenvalue (green circles) is also stable across iterations, and one can get a good estimation of the first excited state. These results are obtained from the two point correlation functions computed with overlap valence quarks on the $N_f = 2 + 1 + 1$ HISQ lattice ensembles with the specifications, $L^3 \times T$ (lattice spacing a in fm) $\equiv 32^3 \times 96$ (0.0888) (top), $48^3 \times 144$ (0.0582) (middle), and $64^3 \times 192$ (0.0441) (bottom) [27, 28], and was discussed in Refs. [8, 29, 30]. In Fig. 8, we present similar results using the HISQ action for valence quarks on the same set of lattices. We show the effective mass and the first two/three TGEVP-eigenvalues of charmonia states. Left panel represents the $J^P \equiv 0^-$ state while the right one corresponds to 1^- and 1^+ states. In this case 1^- requires special attention due to oscillating contributions in the temporal direction. To address that, we employ the smoothed effective mass technique for the ground state of J/ψ , as described in [31]. From the non-oscillating part of

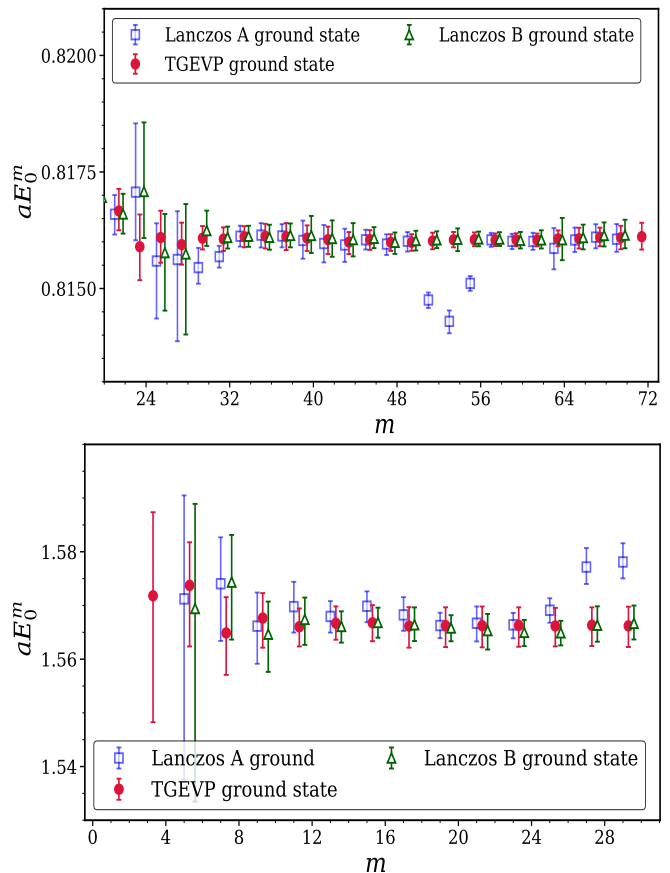


FIG. 6. Comparison of eigenvalues determined by Lanczos and TGEVP methods. Lanczos A is the method as in Ref. [1], Lanczos B utilizes the original Lanczos method [1] but with mean and errors estimated using 68th-percentile, as in the TGEVP method.

the correlators we extract the lowest two eigenvalues which correspond to the masses of $J/\psi(1S)$ and $J/\psi(2S)$ states. The lowest eigenvalue corresponding to the oscillating part of the correlator is also extracted and identified that with the mass of $\chi_{c1}(1P)$ state. For the eigenvalue of the oscillating state, only the negative eigenvalues, $\lambda_n^{m,b}$, of Eq. (9) are retained and then we follow the same analysis procedure as in Sec. (II A).

Based on these results on the lowest two/three eigenstates we then calculate various energy splittings between them, for example, hyperfine splitting in 1S, along with 2S–1S and 1P–1S splittings in charmonia. Since we could extract these values at multiple lattice spacings we then extrapolate them to the continuum limit. Since both the overlap and HISQ actions do not have $\mathcal{O}(n \times ma)$ errors (n odd integers, ma being quark mass in lattice unit), we extrapolate these energy splittings with a fit ansatz, $f(a) = c_1 + c_2 a^2 + c_3 a^4$. We show the continuum extrapolated results in Figs. [9,10, 11]. Fig. 9 represents the hyperfine splitting for 1S-charmonia obtained with both overlap (red square) and HISQ (blue square) actions. The continuum extrapolated results are shown by the red and

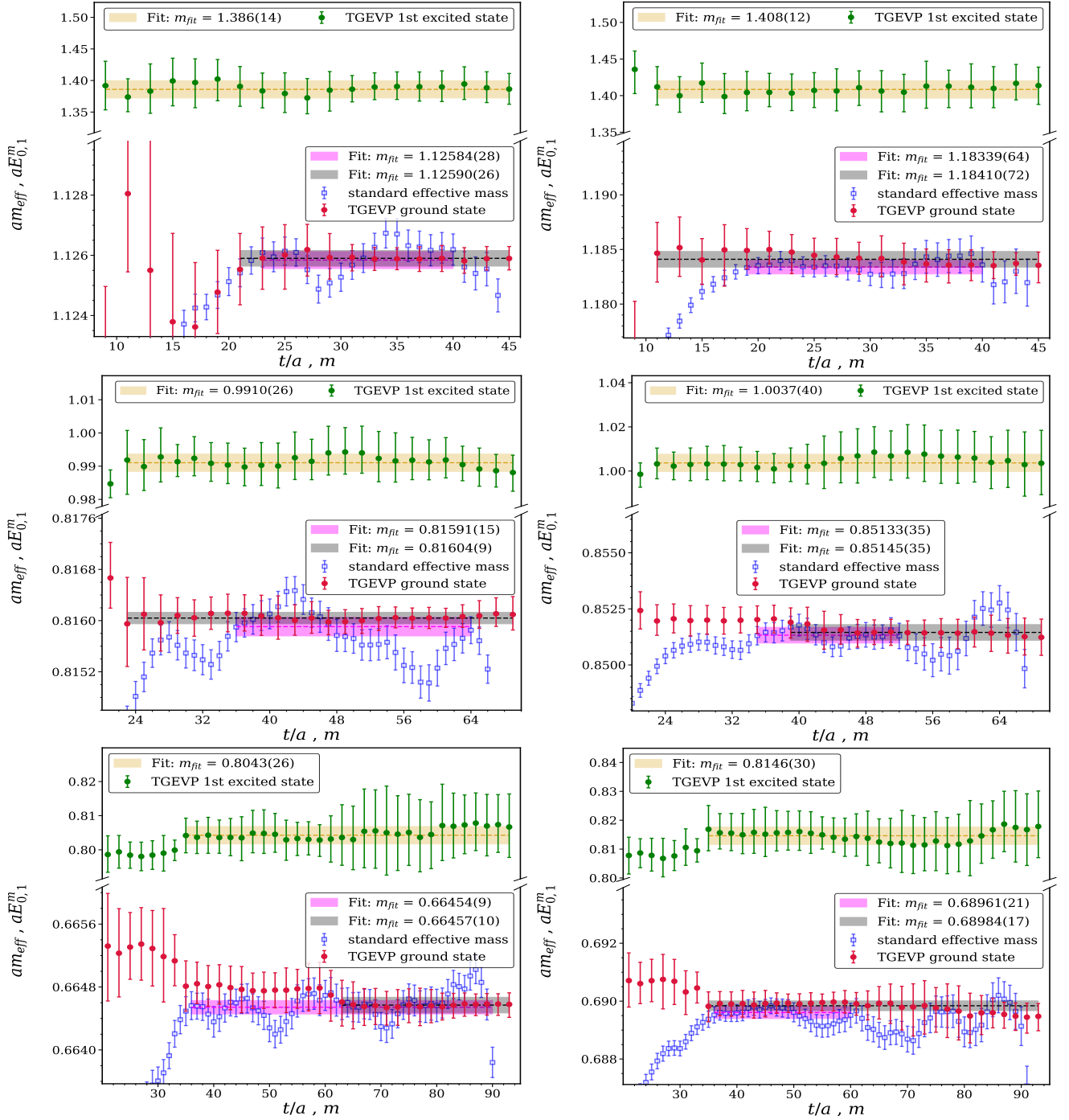


FIG. 7. These plots represent the regular effective mass and the first two TGEVP-eigenvalues corresponding to 1S-charmona states. Left panel is for 0^- and the right one corresponds to 1^- . These results are obtained with overlap valence quarks on the $N_f = 2 + 1 + 1$ HISQ lattice ensembles with the specifications, $L^3 \times T$ (lattice spacing a in fm), $n_{\text{meas}} \equiv$ Top: $32^3 \times 96$ (0.0888), 169, Middle: $48^3 \times 144$ (0.0582), 180, and Bottom: $64^3 \times 192$ (0.0441), 142.

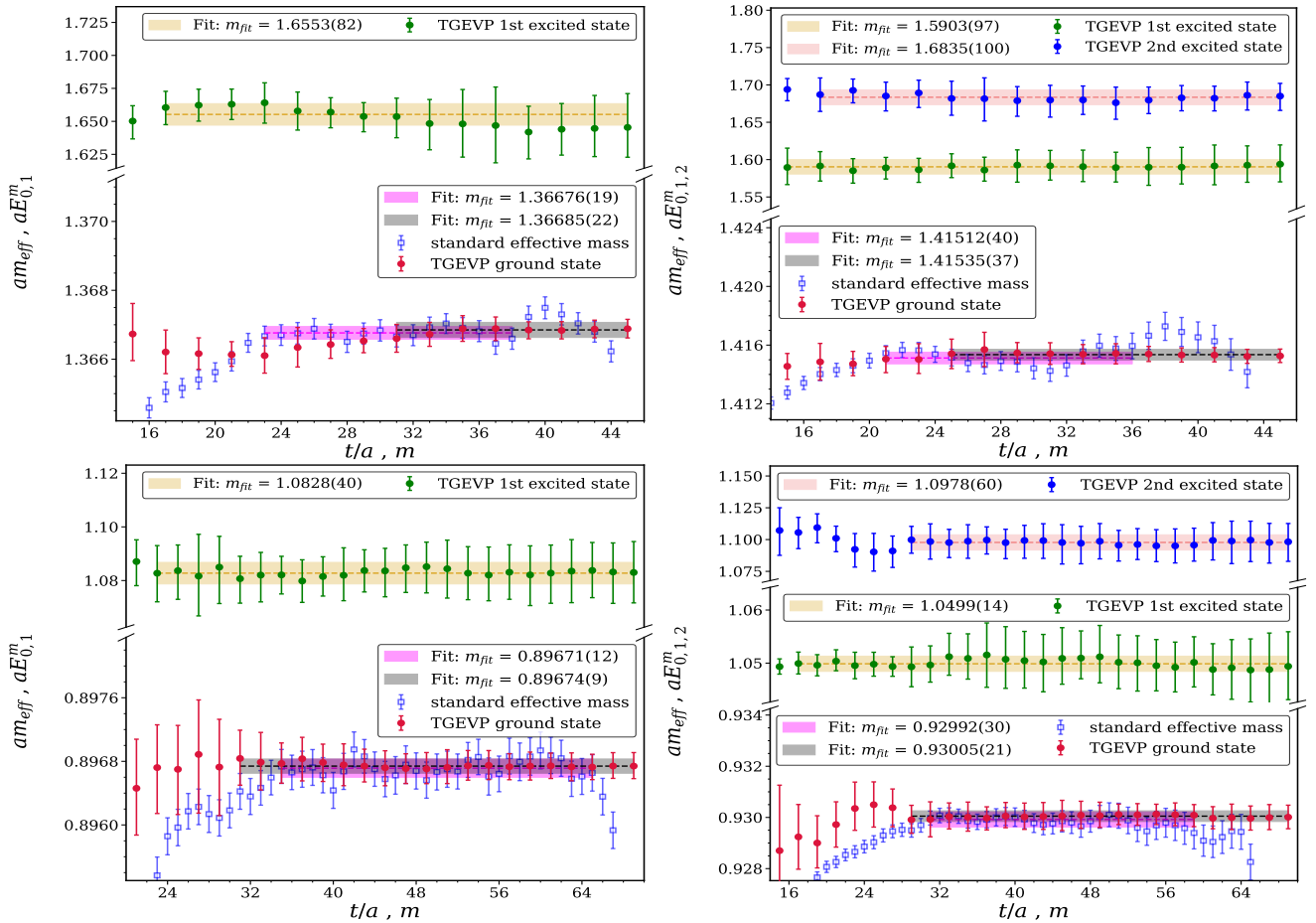


FIG. 8. These plots represent the regular effective mass and the first two (left)/three (right) TGEVP-eigenvalues of charmonia states. Left panel is for $J^P \equiv 0^-$ and the right one corresponds to 1^- together with 1^+ states. These results are obtained with HISQ valence quarks on the $N_f = 2 + 1 + 1$ HISQ lattice ensembles; [Top: $32^3 \times 96$ ($a = 0.0888$) ($n_{meas} = 396$), bottom: $48^3 \times 144$ ($a = 0.0582$) fm ($n_{meas} = 386$).]

green star-symbols respectively, while the experimental value is shown by the magenta square. In Fig. 10, we present the $2S - 1S$ splitting with overlap results at the top and the HISQ results at the bottom pane. Here again, we use the same fit form and extrapolations are shown with the same symbols as above. In Fig. 11, we show the $1P - 1S$ splitting.

These results collectively demonstrate that the TGEVP method can reliably extract not only the ground state but also the excited state spectra from a single correlator. With increased statistics, the precision of excited state measurements can further be improved. This highlights the potential of TGEVP, particularly when combined with multiple operators, to provide highly reliable results for both ground and excited states in lattice QCD calculations.

In Fig. 12, we present the second eigenvalue corresponding to the nucleon correlator that was shown in Fig. 3. Here we plot them together. Note that this second energy level may correspond to the Roper resonance. It needs to be seen if this second energy level can be extracted

robustly at the lighter pion mass, in the presence of $N\pi$ $N\pi\pi$ states, leading to the physical Roper resonance.

In Fig. 13, we present results for nuclei (similar to Fig. 4) but for the case with $m_u = m_d = m_c$. Here we show results for ${}^7\text{Li}$ also. Again for each case we find the TGEVP eigenvalues are much more reliable compared to the fluctuating effective mass. For the cases of ${}^4\text{He}$ and ${}^7\text{Li}$, we observe that the lowest GEVP eigenvalue plateau is somewhat lower than the probable effective mass plateau. That leads to the following question: Whether this is because of the presence of a large number of close-by states, which becomes denser at the higher quark masses, TGEVP fails or the effective mass in this asymmetric source-sink setup becomes quite unreliable? This is an interesting observation and needs to be investigated when more statistics become available.

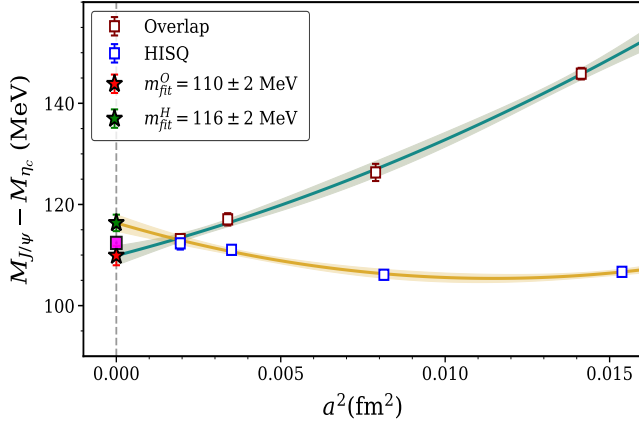


FIG. 9. Hyperfine splitting of 1S-charmonia as extracted from the lowest eigenvalues of 1^- and 0^- correlators, on different lattice ensembles. The data point with red-square (coming from above) are obtained with overlap valence quarks and those with blue-square are due to HISQ valence quarks. Continuum extrapolated results are shown by star-symbols along its physical value (solid magenta square).

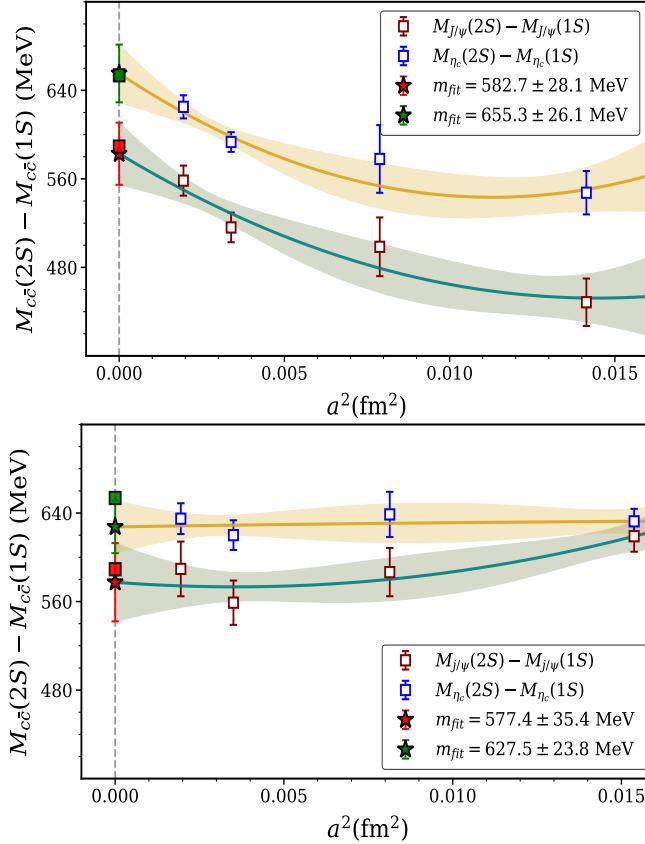


FIG. 10. Continuum extrapolation of the charmonia energy splittings, using the lowest two eigenvalues, obtained by TGEVP method as shown in 7. Top: results with overlap valence quarks, Bottom: same with HISQ valence quarks. The star symbols represent the continuum extrapolated values while solid squares are their experimental values.

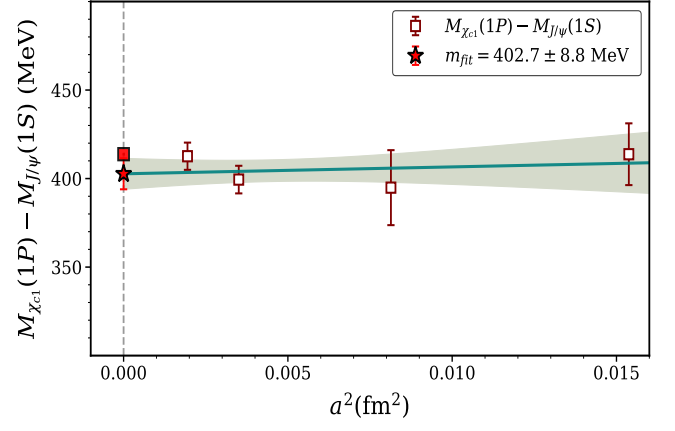


FIG. 11. Continuum extrapolation of the energy splittings, 1P-1S, in charmonia, using the 1st and 3rd eigenvalues as shown in the right pane of Fig. 8.

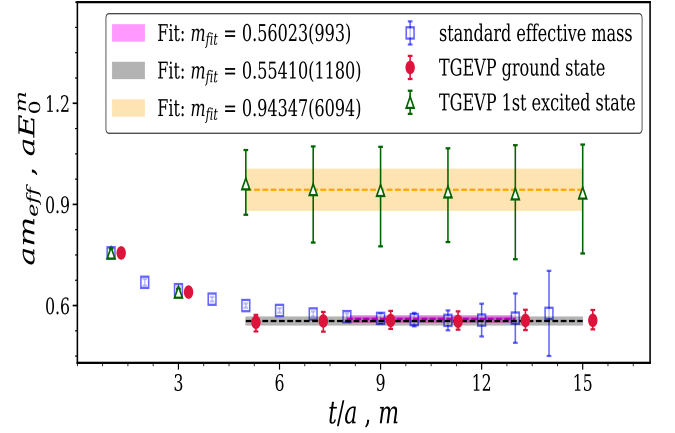


FIG. 12. Second energy level together with the lowest level corresponding to the nucleon correlators shown earlier in Fig. 3. Note the second level may correspond to the Roper resonance.

Appendix D: Detecting peaks from the histograms of eigenvalues

Due to presence of statistical noises spurious eigenvalues appear and that skew their distribution. For a physical state the eigenvalue distribution should have a peak with a width. Hence, the primary objective in detecting peaks from the histograms of eigenvalues is to identify the centers and widths of all peaks present in the histogram. To mitigate the influence of false peaks caused by statistical fluctuations in the data, we begin by smoothing the histogram counts using a Gaussian filter. In a smoothed histogram it becomes easier to detect all peaks that exceed a predefined threshold count. In Fig. 14 we show two such peaks after Gaussian filtering of the original data. This data corresponds to the two-point correlation function of the 1^- states in charmonia and represents the two states showed in the bottom right pane of Fig. 7, $J/\psi(1S)$ and $J/\psi(2S)$.

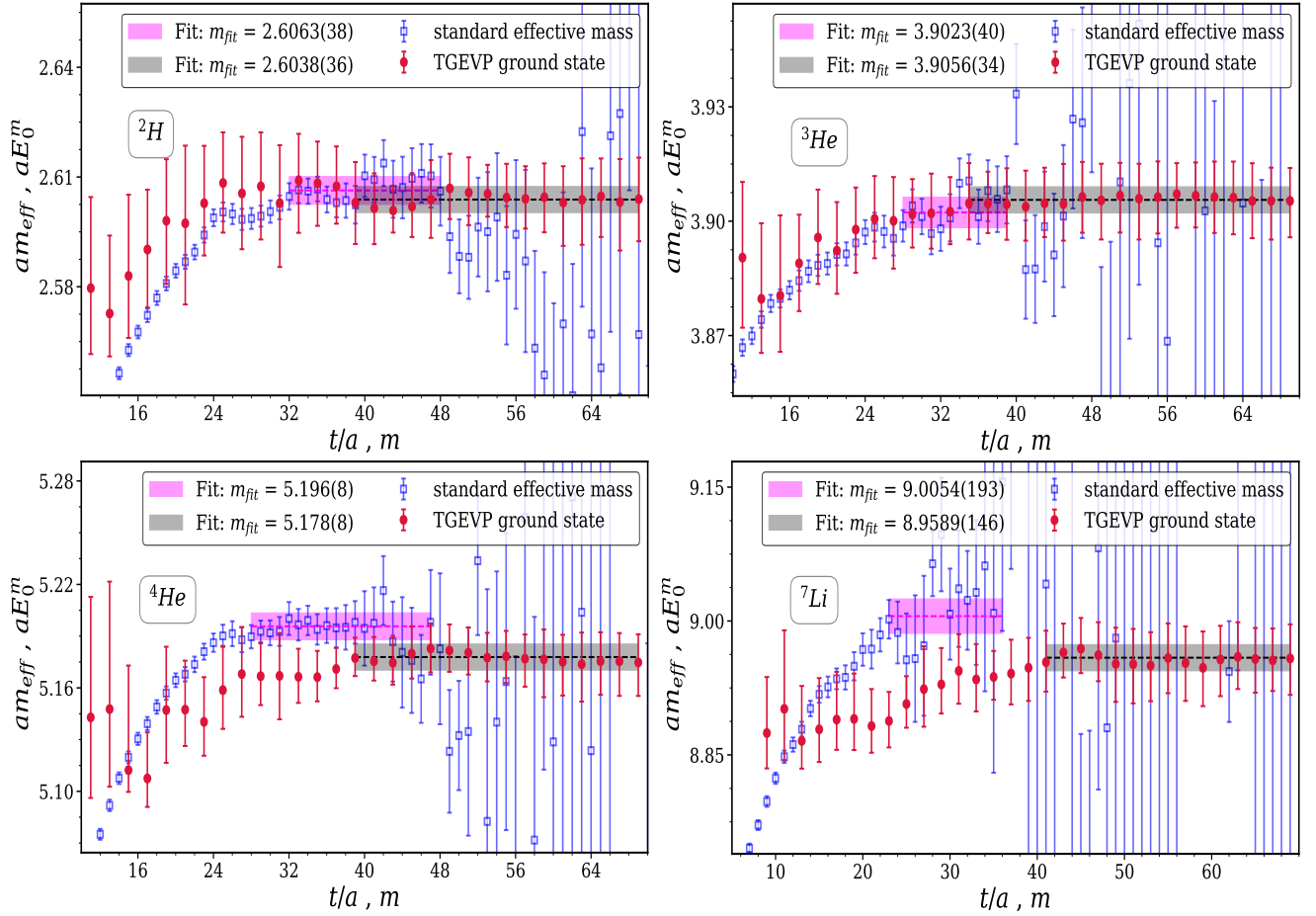


FIG. 13. Lowest energy eigenvalues of a few light nuclei, up to ${}^7\text{Li}$, computed from their two-point functions with the quark masses $m_u = m_d = m_c$. Respective effective masses are also shown for comparison.

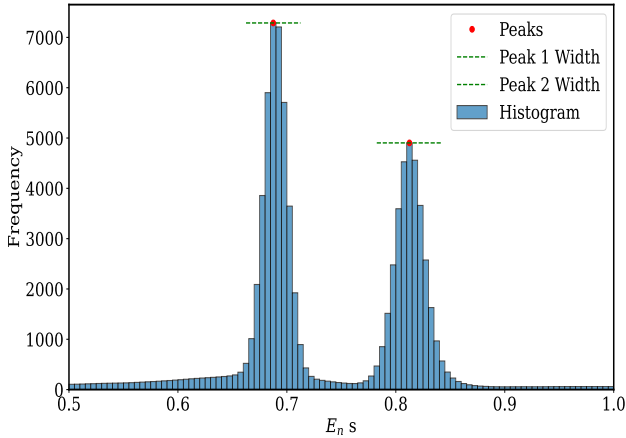


FIG. 14. Histogram plots showing two peaks as determined after Gaussian filtering as described in the text. This data corresponds to the two-point correlation function of the 1^- states in charmonia and represents the two states showed in the bottom right pane of Fig. 7, $J/\psi(1S)$ and $J/\psi(2S)$.

Appendix E: Correlation in TGEVP eigenvalues

The eigenvalues obtained in different iterations of the TGEVP method are inherently correlated, as each iteration builds upon the results of the previous one through random sampling. To assess the extent of this correlation, we compute the associated correlation matrix using the bootstrap method from the eigenvalues that fall within the 68th percentile interval. The first construct the covariance matrix as,

$$\text{Cov}(E_n^i, E_n^j) = \frac{1}{\tilde{N} - 1} \sum_{b=1}^{\tilde{N}} \left(E_n^{(i,b)} - \bar{E}_n^i \right) \left(E_n^{(j,b)} - \bar{E}_n^j \right), \quad (\text{E1})$$

where $E_n^{(i,b)}$ and $E_n^{(j,b)}$ are the b -th bootstrap samples for n -th energy eigenvalues at the i and j -th TGEVP iterations, and \bar{E}_n^i and \bar{E}_n^j are their respective bootstrap means. In Eq. (E1), \tilde{N} is the number of bootstrap samples for which the energy eigenvalues, $E_n^{(i,b)}$ and $E_n^{(j,b)}$, fall within the 68th percentile. The normalized correlation

matrix is then constructed as,

$$\text{Corr} [E_n^i, E_n^j] = \frac{\text{Cov}(E_n^i, E_n^j)}{\sqrt{\text{Cov}(E_n^i, E_n^i) \text{Cov}(E_n^j, E_n^j)}}. \quad (\text{E2})$$

We present here this correlation matrix in a color-coded format for a few eigenvalues presented in the main text. In Fig. 15, we show a plot showing correlation matrix corresponding to the excited state of 1^- state in charmonia. This corresponds to the second eigenvalue of the top right plot of Fig. 7. As can be seen that correlation is somewhat larger compared to that of the lowest eigenvalues shown in Fig. 5. The higher eigenvalues corresponding to other correlation functions also show the same pattern of higher correlation than that present in the lowest eigenvalue. In Fig. 16 we depict the correlation matrix plot of the first two eigenvalues of the nucleon two-point functions corresponding to the two states shown in Fig. 12. Here again, the second state, which may correspond to the Roper resonance, shows more correlation than the ground state.

In Fig. 17 we show correlation matrix for the light nuclei. The top pane corresponds to deuteron correlators at $m_u = m_d = m_s$ (left) and $m_u = m_d = m_c$ (right), respectively. The bottom pane represents the same for ${}^4\text{He}$. It clearly shows that correlation increases at the lighter quark mass and also increases with the atomic number. The eigenvalues corresponding to ${}^4\text{He}$ correlators at the strange quark mass are correlated to a large extent, and increases further as the quark mass become lighter.

This analysis leads us to the following observations: 1. If the statistics is high and the effective mass is reasonably good we do not find much correlation of eigenvalues across iterations. In that case fitting these eigenvalues with a constant term will be reliable and provide better estimate compared to exponential fitting. This could be a good choice in multi-operator GEVP setup, that is merging of GEVP and TGEVP together. We will explore that in future 2. For the higher eigenvalues, correlations are larger than that for the case of lowest eigenvalue. With higher statistics we find the correlation in the higher eigenvalues also decreases. 3. For multi-nucleons we find correlations to be higher than the single nucleon. This is a concern and needs to be addressed properly in a multinucleon calculation, particularly considering the presence of dense spectrum. It remains to be seen how this correlation evolves with higher statistics in these systems.

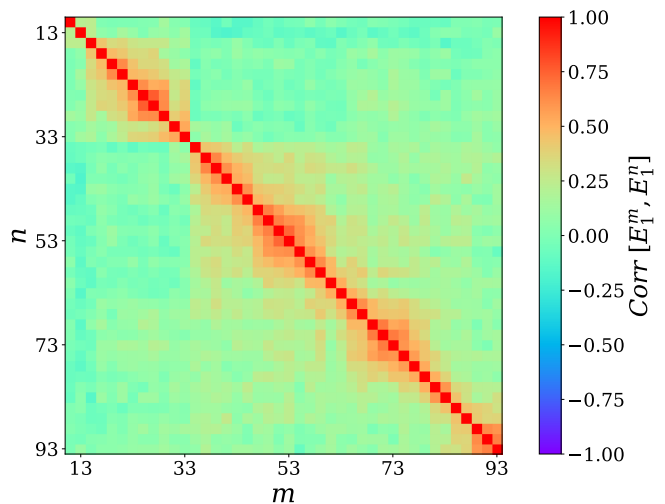


FIG. 15. Correlation matrix plot corresponding to the second eigenvalue of the two-point correlation function of 1^- state in charmonia ($J/\psi(2S)$ state.)

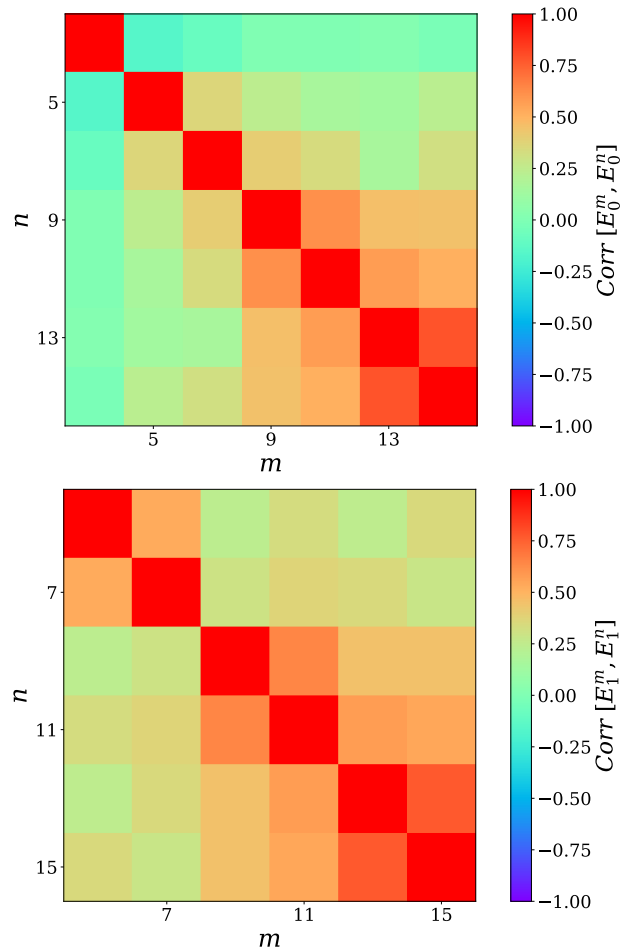


FIG. 16. Correlation matrix plot for the first two eigenvalues of the nucleon correlators corresponding to the two states shown in Fig. 12.

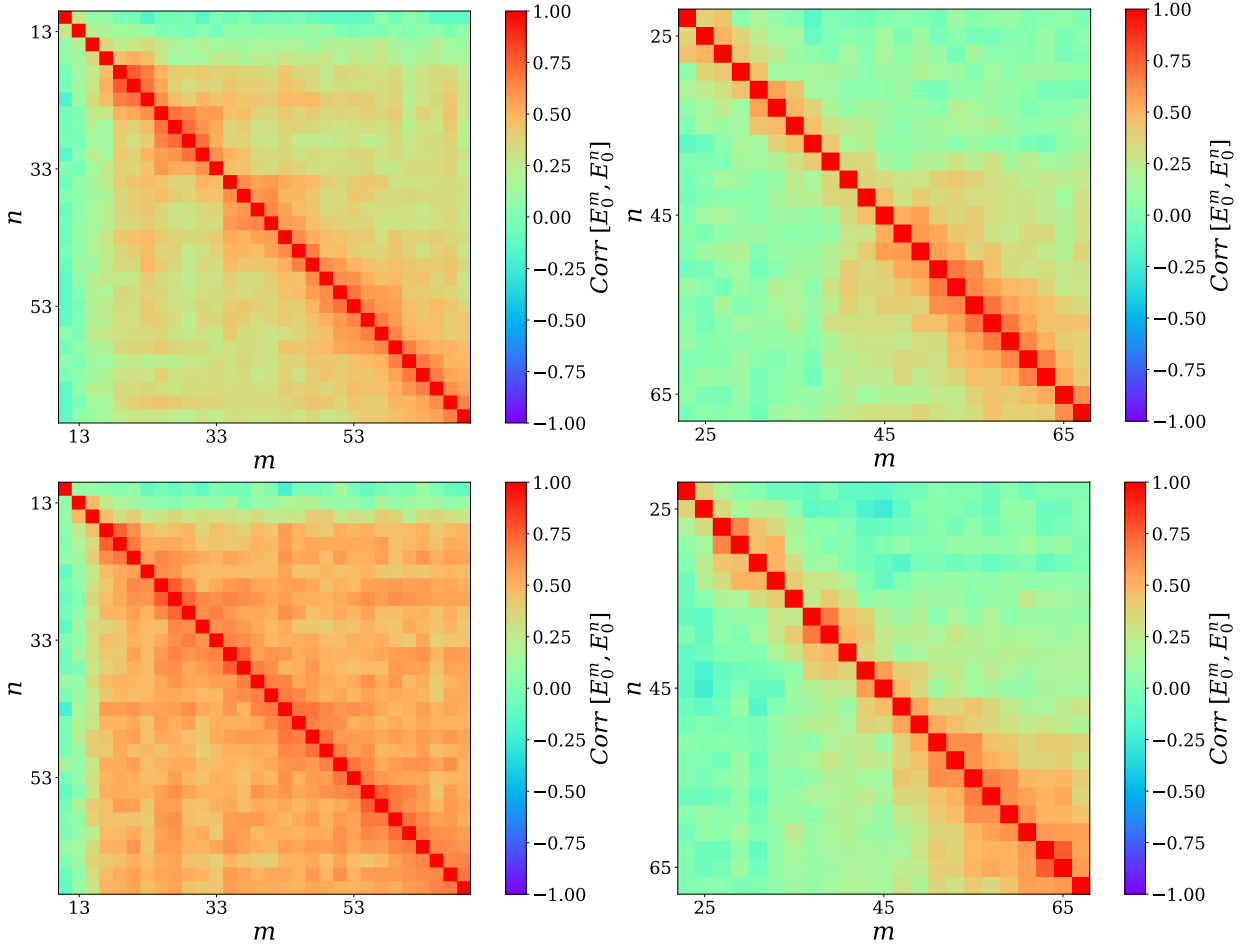


FIG. 17. Correlation matrix plot corresponding to the lowest eigenvalues of ${}^2\text{H}$ and ${}^4\text{He}$. The top pane corresponds to ${}^2\text{H}$ computed with the quark masses $m_u = m_d = m_s$ (left) and $m_u = m_d = m_c$ (right), respectively. The bottom pane represents the same for ${}^4\text{He}$.

-
- [1] M. L. Wagman, Lanczos, the transfer matrix, and the signal-to-noise problem, [arXiv: 2406.20009 \(2024\)](#).
- [2] C. Michael, Adjoint sources in lattice gauge theory, *Nuclear Physics B* **259**, 58 (1985).
- [3] M. Luscher and U. Wolff, How to Calculate the Elastic Scattering Matrix in Two-dimensional Quantum Field Theories by Numerical Simulation, *Nucl. Phys.* **B339**, 222 (1990).
- [4] S. Dürr, Z. Fodor, J. Frison, C. Hoelbling, R. Hoffmann, S. D. Katz, S. Krieg, T. Kurth, L. Lellouch, T. Lippert, K. K. Szabo, and G. Vulvert, Ab initio determination of light hadron masses, *Science* **322**, 1224 (2008).
- [5] C. T. H. Davies *et al.* (HPQCD, UKQCD, MILC, Fermilab Lattice), High precision lattice QCD confronts experiment, *Phys. Rev. Lett.* **92**, 022001 (2004).
- [6] R. J. Dowdall, C. T. H. Davies, T. C. Hammant, and R. R. Horgan (HPQCD Collaboration), Precise heavy-light meson masses and hyperfine splittings from lattice qcd including charm quarks in the sea, *Phys. Rev. D* **86**, 094510 (2012).
- [7] Z. S. Brown, W. Detmold, S. Meinel, and K. Orginos, Charmed bottom baryon spectroscopy from lattice QCD, *Phys. Rev. D* **90**, 094507 (2014).
- [8] N. Mathur, M. Padmanath, and S. Mondal, Precise predictions of charmed-bottom hadrons from lattice QCD, *Phys. Rev. Lett.* **121**, 202002 (2018).
- [9] R. A. Briceño, J. J. Dudek, and R. D. Young, Scattering processes and resonances from lattice qcd, *Rev. Mod. Phys.* **90**, 025001 (2018).
- [10] G. Parisi, The strategy for computing the hadronic mass spectrum, *Physics Reports* **103**, 203 (1984).
- [11] G. P. Lepage, The analysis of algorithms for lattice field theory, Invited lectures given at TASI'89 Summer School, Boulder, Published in Boulder ASI 1989:97-120 (QCD161:T45:1989) (1989).
- [12] W. Detmold and K. Orginos, Nuclear correlation functions in lattice qcd, *Phys. Rev. D* **87**, 114512 (2013).
- [13] W. Detmold and M. G. Endres, Signal/noise enhancement strategies for stochastically estimated correlation functions, *Phys. Rev. D* **90**, 034503 (2014).
- [14] M. Cè, L. Giusti, and S. Schaefer, Domain decomposition, multilevel integration, and exponential noise reduction in lattice qcd, *Phys. Rev. D* **93**, 094507 (2016).
- [15] D. Chakraborty, P. Srivastava, A. Kumar, and N. Mathur, Nuclear correlation functions using first-principle calculations of lattice quantum chromodynamics, [2411.08962 \(2024\)](#).
- [16] D. C. Hackett and M. L. Wagman, Lanczos for lattice QCD matrix elements, [arXiv: 2407.21777 \(2024\)](#).
- [17] S. Kaniel, Estimates for some computational techniques in linear algebra, *Mathematics of Computation* **20**, 369 (1966).
- [18] Y. Saad, On the rates of convergence of the lanczos and the block-lanczos methods, *SIAM Journal on Numerical Analysis* **17**, 687 (1980).
- [19] J. Ostmeier, A. Sen, and C. Urbach, On the equivalence of Prony and Lanczos methods for Euclidean correlation functions, [arXiv: 2411.14981 \(2024\)](#).
- [20] B. G. R. de Prony, Essai experimental et analytique: sur les lois de la dilatabilité e de fluides elastique et sur celles de la force expansive de la vapeur de l'alkool, a différentes temp eratures,, *Journal de l'école polytechnique*, **1(22)**, 24 (1975).
- [21] G. T. Fleming, What can lattice QCD theorists learn from NMR spectroscopists?, in *3rd International Workshop on Numerical Analysis and Lattice QCD* (2004) pp. 143–152, [arXiv:hep-lat/0403023](#).
- [22] S. Kunis, T. Peter, T. Roemer, and U. von der Ohe, A multivariate generalization of prony's method, *arXiv: Numerical Analysis* (2015).
- [23] M. Fischer, B. Kostrzewa, J. Ostmeier, K. Ottnad, M. Ueding, and C. Urbach, On the generalised eigenvalue method and its relation to prony and generalised pencil of function methods, *The European Physical Journal A* **56**, 206 (2020).
- [24] J. Cullum and R. A. Willoughby, Computing eigenvalues of very large symmetric matrices—an implementation of a lanczos algorithm with no reorthogonalization, *Journal of Computational Physics* **44**, 329 (1981).
- [25] SciPy-community, `scipy.linalg.eig`, **1.14.1 (stable)** (2024).
- [26] E. Polizzi, Density-matrix-based algorithm for solving eigenvalue problems, *Phys. Rev. B* **79**, 115112 (2009).
- [27] A. Bazavov *et al.* (MILC), Lattice QCD Ensembles with Four Flavors of Highly Improved Staggered Quarks, *Phys. Rev. D* **87**, 054505 (2013).
- [28] A. Bazavov *et al.*, *B*- and *D*-meson leptonic decay constants from four-flavor lattice QCD, *Phys. Rev. D* **98**, 074512 (2018).
- [29] N. Mathur and M. Padmanath, Lattice qcd study of doubly charmed strange baryons, *Phys. Rev. D* **99**, 031501 (2019).
- [30] N. S. Dhindsa, D. Chakraborty, A. Radhakrishnan, N. Mathur, and M. Padmanath, Precise study of triply charmed baryons (Ω_{ccc}), [arXiv: 2411.12729 \(2024\)](#).
- [31] C. DeTar and S.-H. Lee, Variational method with staggered fermions, *Phys. Rev. D* **91**, 034504 (2015).